



OPEN

A role for the periplasmic adaptor protein AcrA in vetting substrate access to the RND efflux transporter AcrB

Ilyas Alav¹, Vassiliy N. Bavro²✉ & Jessica M. A. Blair¹✉

Tripartite resistance-nodulation-division (RND) efflux pumps, such as AcrAB-TolC of *Salmonella* Typhimurium, contribute to antibiotic resistance and comprise an inner membrane RND-transporter, an outer membrane factor, and a periplasmic adaptor protein (PAP). The role of the PAP in the assembly and active transport process remains poorly understood. Here, we identify the functionally critical residues involved in PAP-RND-transporter binding between AcrA and AcrB and show that the corresponding RND-binding residues in the closely related PAP AcrE, are also important for its interaction with AcrB. We also report a residue in the membrane-proximal domain of AcrA, that when mutated, differentially affects the transport of substrates utilising different AcrB efflux channels, namely channels 1 and 2. This supports a potential role for the PAP in sensing the substrate-occupied state of the proximal binding pocket of the transporter and substrate vetting. Understanding the PAP's role in the assembly and function of tripartite RND pumps can guide novel ways to inhibit their function to combat antibiotic resistance.

Antibiotic resistance is one of the greatest global public health challenges and threatens our ability to effectively treat and prevent infectious diseases¹. In clinical isolates of Gram-negative bacteria, the Resistance-Nodulation-Division (RND) family of efflux pumps are frequently upregulated and associated with multidrug-resistant phenotypes^{2–6}. Tripartite RND pumps span the double membrane of Gram-negative bacteria and consist of an inner membrane RND transporter, a periplasmic adaptor protein (PAP), and an outer membrane factor (OMF)^{7,8}. The AcrAB-TolC pump is the principal RND efflux system in Enterobacteriaceae, including *Salmonella enterica*. It can export a wide range of structurally different compounds, including clinically relevant antibiotics such as β -lactams and fluoroquinolones^{9,10}.

Gram-negative bacteria encode a wide repertoire of RND transporters, which typically pair with a single cognate PAP and an OMF to form tripartite pumps that have varied substrate specificities and physiological roles^{10–16}. The *S. enterica* genome encodes five RND pumps: AcrAB-TolC, AcrEF-TolC, AcrAD-TolC, MdtABC, and MdsABC¹⁰. The AcrEF-TolC pump possesses a similar substrate profile to AcrAB-TolC, but its expression is silenced by H-NS under laboratory conditions¹⁷. The PAPs comprise four domains: α -helical domain, lipoyl domain, β -barrel domain and the membrane-proximal domain (MPD)¹⁸. The α -helical domain has a coiled-coil arrangement and appears to interact with the α -barrel domain of the OMF^{18,19}. The lipoyl domain is involved in stabilising the self-assembly of the PAPs within the tripartite efflux pump. The β -barrel domain is flexibly linked to the MPD, and both domains appear to interact with the porter domain of the RND-transporter²⁰. The MPD of RND-associated PAPs is critical for the assembly and function of AcrAB-TolC in *E. coli* and *S. enterica*^{21,22}. In the PAPs ZneB and CusB of the tripartite ZneCAB and CusABC RND efflux pumps, respectively, the MPD appears to play an important role in substrate acquisition and presentation to the metal pumping RND transporters^{23,24}. Additionally, in the related ABC-transporter-associated PAP MacA, the MPD has been demonstrated to be involved in direct binding of possible pump substrates²⁵ and has been suggested to be involved in substrate vetting¹⁸.

Previous studies have shown that AcrA and AcrE are interchangeable in *S. enterica*^{22,26,27}, whereas MdtA and MdsA can only function with their cognate RND-transporters²². Previously, we showed that the regions of PAP-transporter contact are relatively compact and discrete. Based on homology models of the PAPs in *Salmonella*,

¹Institute of Microbiology and Infection, College of Medical and Dental Sciences, University of Birmingham, Birmingham B15 2TT, UK. ²School of Life Sciences, University of Essex, Colchester CO4 3SQ, UK. ✉email: v.bavro@essex.ac.uk; j.m.a.blair@bham.ac.uk

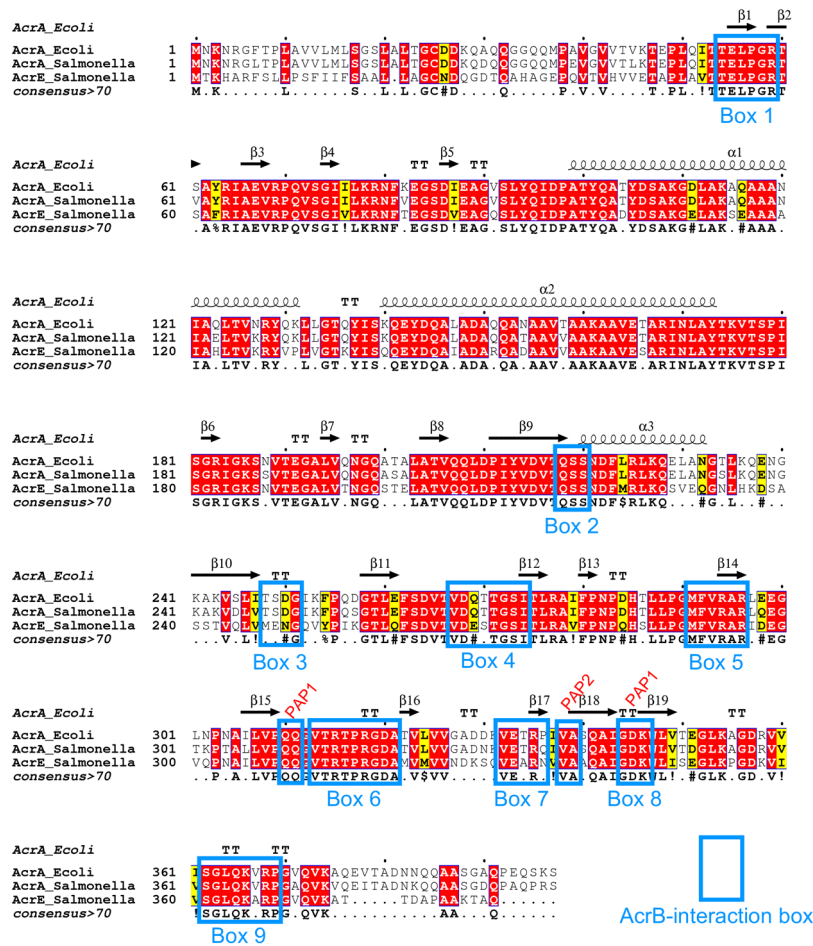


Figure 1. Multiple sequence alignment of *Salmonella* AcrA and AcrE combined with the mapping of the secondary structure derived from the experimentally defined structure of *E. coli* AcrA (PDB 5V5S, chain G)²⁰. Identical residues are coloured red and similar residues are coloured yellow. The PAP-binding boxes implicated in RND-binding²² are numbered 1 to 9 and depicted using blue rectangles. Figure created using Esprict 3.0⁴⁷.

we found these regions to be highly conserved between AcrA and AcrE, while differing significantly between divergent PAPs, such as MdtA and MdsA, providing a possible explanation of the observed interoperability of AcrA and AcrE. The 3D RND-interaction sites can be delineated into discrete linear sequences, which we have dubbed “binding boxes”, that map to the β -barrel domain (boxes 1–5) and the MPD (6–9). Disruption of a few key residues within the binding boxes 1 and 4–6 mapping to the exposed β -barrel loops and the MPD, abrogated transport, suggesting an important role for this region in AcrB-binding²².

Here, we set out to further validate the “binding box” model of PAP-RND interaction by phenotypic profiling of site-directed mutations targeting the β -barrel and membrane-proximal domains. We specifically sought to describe the efflux profiles of substrates that have been suggested to utilise different AcrB efflux channels^{28–30}.

Results

Refining the binding box model of PAP-RND interactions. Previously, using disruptive site-directed mutagenesis (SDM), we demonstrated discrete stretches of residues, which we dubbed “binding boxes” based on their spacial proximity^{19,20,31,32}, control PAP-RND complex formation and recognition of cognate PAP-RND pairs²². Here, we set out to refine our binding box model by generating and testing the effects of more subtle and conservative mutations to identify the PAP-residues most critical for RND-binding (Fig. 1). Specifically, residues that were previously shown to be important for RND-binding²² were mutated to residues with similar properties to produce conservative mutations, while residues, the previous mutation of which led to limited functional impact were subjected to more disruptive mutagenesis. Mutated versions of AcrA were expressed in the *Salmonella* Typhimurium SL1344 Δ 4PAP strain, which lacks all four known RND-associated PAPs (AcrA, AcrE, MdtA and MdsA)²². The effects of the mutations on efflux function were assessed using ethidium bromide efflux assays and antimicrobial susceptibility testing.

The PAPs reside in the periplasm and are embedded in the plasma membrane by a lipid anchor and/or a transmembrane helix and are composed of several well-defined domains^{18,33}. From the plasma membrane outward, these are the MPD (containing boxes 6–9), the β -barrel domain (containing boxes 1–5), the lipoyl

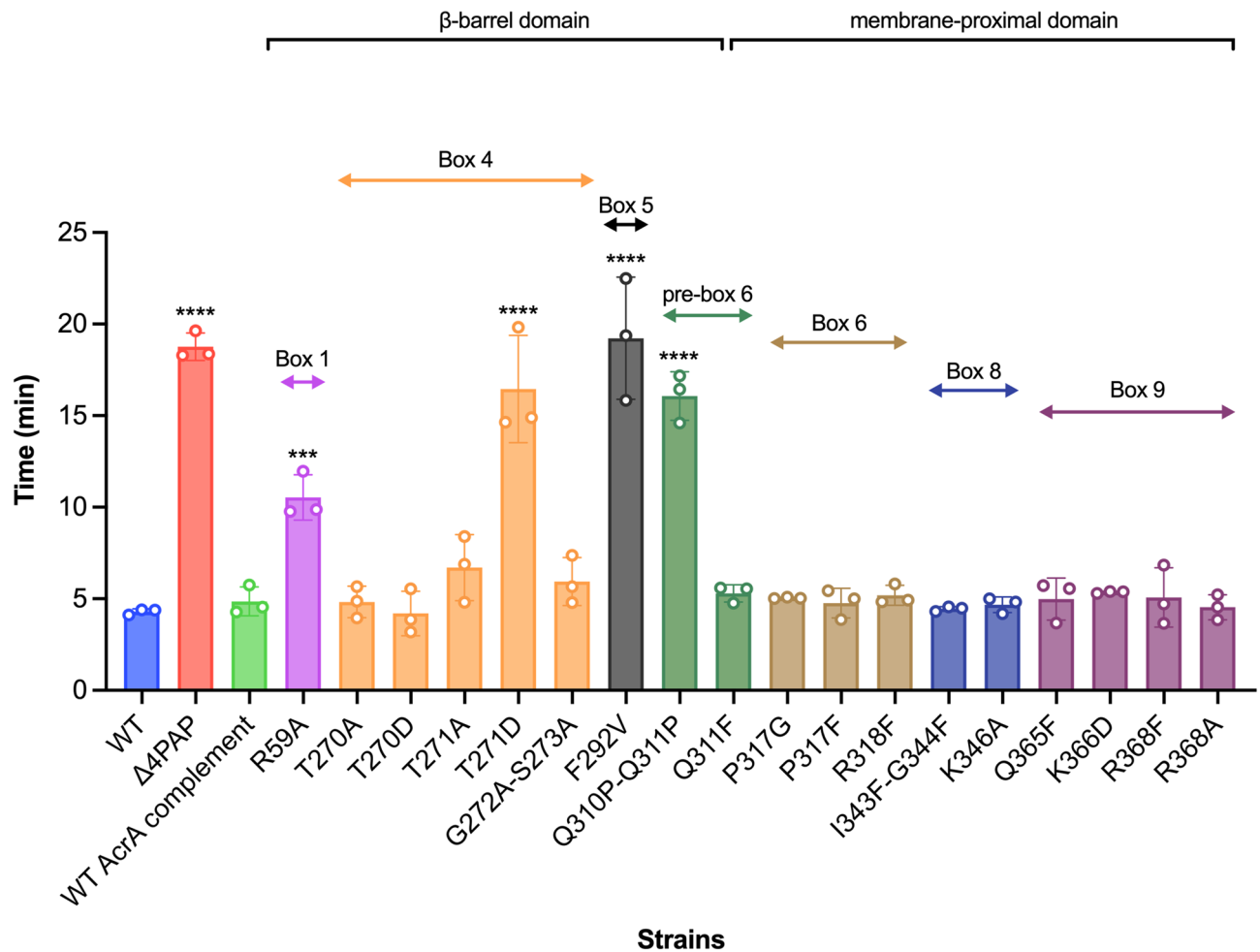


Figure 2. Efflux of ethidium bromide by the *Salmonella* Typhimurium SL1344 Δ 4PAP strain complemented with mutated versions of AcrA. Data presented are the mean of three biological replicates and are shown as the time taken for the fluorescence to decrease by 25% \pm standard deviation. Bacteria were treated with ethidium bromide and the proton-motive force dissipator CCCP for 1 h and then re-energised with glucose. The annotation above indicates the mapping of each mutation to its binding box and the domain mapping of respective boxes. Data were analysed by one-way ANOVA and compared to the WT AcrA complement using Dunnett's test. Strains with significantly different efflux are indicated with *** ($P \leq 0.001$) or **** ($P \leq 0.0001$).

domain, and the α -hairpin domain¹⁸. The G58F mutation mapping to box 1 was previously shown to impair efflux function²². Mutations targeting boxes 2, 3 and 7 did not result in detectable changes in the accumulation or efflux of ethidium bromide²², and in the current study, we focused our attention on further characterisation of the remaining boxes. Here, the R59A mutation was produced to investigate whether other residues in proximity to box 1 had a role in RND-binding. The R59A mutation caused an intermediate impairment of efflux function, between that of the Δ 4PAP and the WT complement strain, confirming the important role of box 1 (Fig. 2 and Table S2). Residues that were mutated as pairs in our previous study were separated to identify the most critical residue. The T270F-T271F mutation mapping to box 4 was separated into T270D and T271D for disruptive mutagenesis, and T270A and T271A as more subtle mutations. The T271D mutation significantly impaired efflux, whilst the T270D mutation had no effect. Furthermore, the T271A mutation still caused a mild impairment of efflux function (Fig. 2 and Table S2), suggesting that T271 is a critical residue in efflux function. The G272P-S273P mutation mapping to box 4 previously impaired efflux function, therefore, a more conservative mutation was produced to determine the role of G272-S273. The G272A-S273A mutation did not affect efflux activity, indicating that these residues can tolerate neutral mutations (Fig. 2 and Table S2). The F292G mutation mapping to box 5 was previously shown to affect both AcrB- and AcrD-binding^{22,27}. Hence, the F292V mutation was produced to determine whether a more subtle change would still affect efflux function. Like the F292G phenotype, the F292V mutation also caused significant impairment of efflux (Fig. 2 and Table S2), indicating that F292 is critical for efflux function. The Q310F mutation mapping to box 6 was previously shown to have no impact on efflux function, and the Q311F reported here, similarly did not influence efflux function detectably (Fig. 2 and Table S2). Therefore, both residues were simultaneously mutated into Q310P-Q311P, which resulted in significant impairment of efflux function, indicating that double glutamine residues may provide some functional redundancy and that the presence of a glutamine residue may be critical in this position (Fig. 2 and Table S2).

Mutations mapping to box 6, including R315F and R318A, were previously shown to have no impact on efflux function. Therefore, several novel mutations mapping to box 6 were produced (P317G, P317F and R318F), which did not have any impact on efflux function (Fig. 2 and Table S2). Novel mutations mapping to box 8 (I344F-G344F and K346A) also had no observable influence on efflux function (Fig. 2 and Table S2). G363 in box 9 was shown by us and other studies to be critical for efflux function^{22,26,27}. Further mutations in box 9 were produced to investigate whether other residues also play a role in RND-binding. However, the Q365F, K366D, R368F and R368A mutations did not affect efflux function, suggesting that only G363 is critical for efflux function (Fig. 2 and Table S2). Western blotting verified that the observed effects of the mutations with impaired efflux were not due to changes in protein expression levels or stability (Fig. S1).

AcrE and AcrA share conserved binding boxes that are responsible for their interoperability relative to AcrB.

The binding boxes between AcrA and AcrE were previously shown to be highly conserved in *Salmonella* Typhimurium (Fig. 1), potentially explaining the observed interchangeability between the two PAPs²². To validate their functional role in AcrE, SDM was used to mutate the residues, corresponding to the most critical binding box residues previously identified in AcrA²²—namely G57, R58, T270, F291, R293 and G362 (Fig. 1). The effect of the mutations was assessed by ethidium bromide accumulation assays and antimicrobial susceptibility testing in the Δ 4PAP Δ acrF strain²². This strain lacks all four RND-associated PAPs and the cognate RND-transporter AcrF, thereby allowing the impact of AcrE mutations on AcrB-binding to be determined. All mutations corresponding to the critical residues of AcrA (AcrE G57F, R58A, T270D, F291G, R293F and G362F) also had a significant effect on efflux function and antimicrobial susceptibility (Fig. 3 and Table S3). Consistent with this, the mutation of phenotypically neutral residues in AcrA, corresponding to the AcrE T216F (mapping to box 2), K365D and R367D (both mapping to box 9) respectively, also had no impact on efflux function (Fig. 3 and Table S3). The observed effects of the mutations tested stemmed from their impact on the function of the protein and were not due to changes in expression levels or stability of the variant alleles, as validated by Western blotting, with a possible exception of G57F (Fig. S1). The above results confirm the conservation of function of the binding boxes between AcrA and AcrE, which explains their interoperability in conjunction with AcrB.

A potential role for the membrane-proximal domain of AcrA in vetting substrate access to channel 1 and channel 2.

The refinement of the binding box model of PAP-RND interaction led to the discovery of an AcrA mutation with a peculiar phenotype. The K366D AcrA mutation mapping to box 9 (Fig. 1), did not alter ethidium bromide efflux or susceptibility (Fig. 2) but showed a distinct antimicrobial susceptibility profile to other antimicrobials tested (Table S2). Notably, the K366D mutation in AcrA conferred differential effects depending on the physicochemical properties of the compounds tested. The K366D AcrA mutation caused a greater than two-fold reduction in MIC values to high-molecular-mass drugs (HMMDs), such as doxorubicin, erythromycin, fusidic acid and novobiocin ($M > 500 \text{ g mol}^{-1}$) and low-molecular-mass drugs (LMMDs), such as chloramphenicol, clindamycin, linezolid, and minocycline ($M < 500 \text{ g mol}^{-1}$), compared to the WT AcrA complement. However, the K366D AcrA mutation had no impact on the MIC values for planar aromatic cations (PACs), including acriflavine, berberine, benzalkonium chloride, crystal violet, ethidium bromide, methylene blue and rhodamine 6G (Table 1).

Previous studies have associated the molecular weight of the substrate-drugs with the preferred channel access and binding pocket validation by the RND-transporter^{28,29,34,35}. The RND-transporter AcrB has multiple substrate entry channels identified, which are used by drugs depending on their physicochemical properties^{28,29,36} (Fig. 4). LMMDs have been proposed to preferentially enter through channel 1 (CH1), whilst HMMDs are thought to enter AcrB through channel 2 (CH2)^{36–38}. The cleft entrance of CH2 has been previously suggested to be impacted by the MPD of AcrA²⁸. This is seen in cryo-EM structures of the AcrAB-TolC complex, which show that AcrA interacts with the PC1 and PC2 subdomains of AcrB^{19,39}. PACs on the other hand, are preferentially taken up through channel 3 (CH3), which starts from the vestibule formed by the central cavity of the three AcrB protomers and leads directly to the deep binding pocket (DBP)²⁸. The entrance of the recently proposed channel 4 (CH4) is in the groove formed by TM1 and TM2 and leads to the DBP³⁰. The location of CH3 and CH4 within AcrB suggests that the MPD of AcrA should not have a direct steric impact on drug access (Fig. 4).

Therefore, to understand how the K366D AcrA mutation affects the susceptibility of the Δ 4PAP strain to HMMDs and LMMDs, but not to PACs, we designed more specific antimicrobial sensitivity screens to be able to better differentiate the usage of the access channels by respective substrates and the impact of the K366D AcrA mutation on specific channels. Doxorubicin has been suggested to utilise CH2 to enter AcrB^{29,34}. Therefore, we analysed the effect of the K366D AcrA mutation on its efflux. We capitalised on the doxorubicin fluorescence outside of the cell to establish the level of efflux (Fig. 5). While the WT AcrA complement and the Q311F AcrA mutation had similar levels of doxorubicin efflux, the F292V and K366D AcrA mutations caused severe impairment of doxorubicin efflux, close to that of the Δ 4PAP negative control. This result suggested that the K366D AcrA mutation has a strong impact on drugs using CH2.

To further clarify the impact of the K366D AcrA mutation on the specific channels, we monitored growth in the presence of efflux-substrates at $0.25 \times \text{MIC}$ for the K366D AcrA mutation, using the efflux-impaired F292V and phenotypically neutral Q311F AcrA mutations as controls. The growth kinetics data showed that compared to the WT AcrA complement, the K366D AcrA mutation caused poor growth in the presence of CH2-substrates doxorubicin, erythromycin, minocycline, and clindamycin (Fig. 6). The K366D AcrA mutation also caused a growth defect in the presence of CH1-substrates, including novobiocin, fusidic acid and chloramphenicol (Fig. 6). Notably, the K366D AcrA mutation did not affect growth in the presence of CH3-substrates, such as ethidium bromide and rhodamine 6G (Fig. 6). This data shows the disproportionate impact of the K366D AcrA mutation

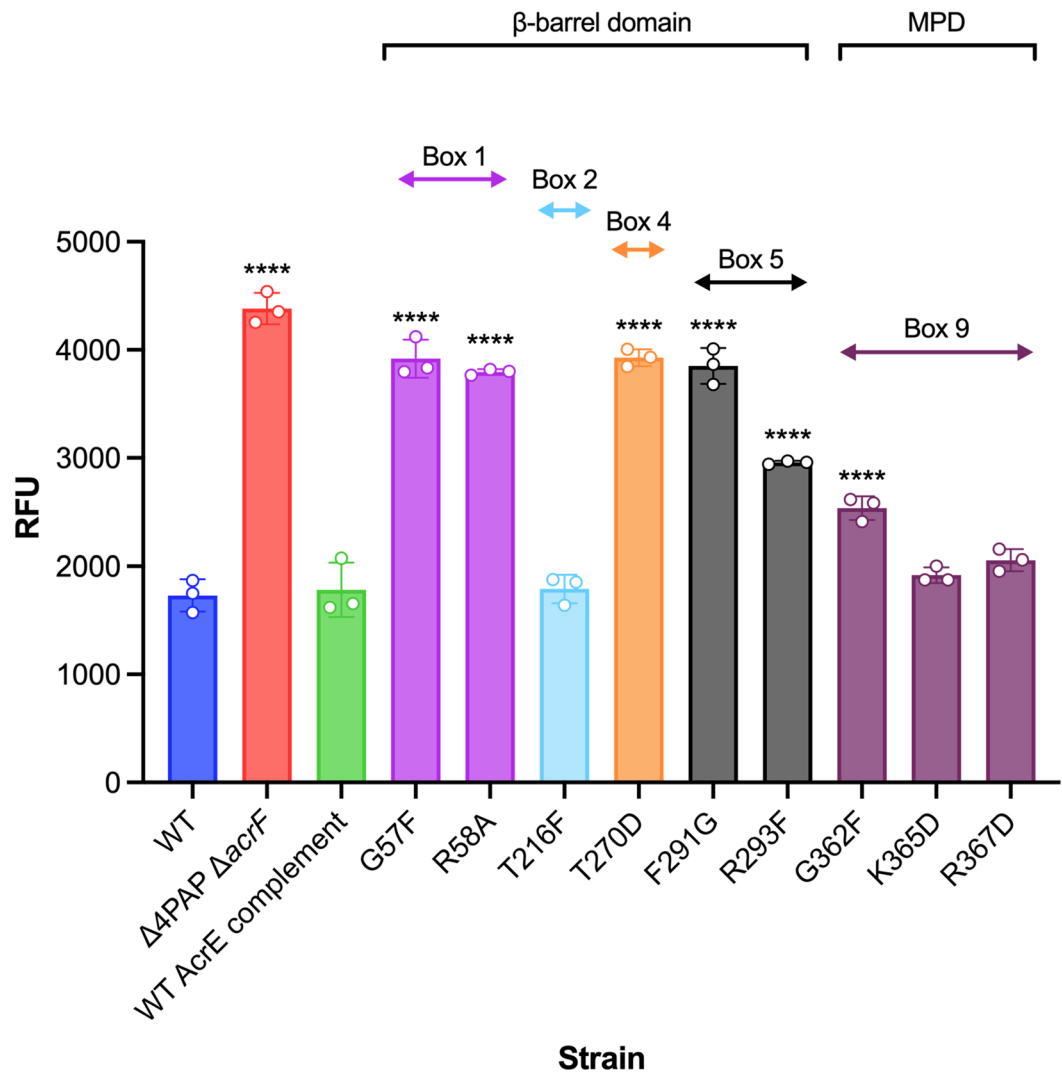


Figure 3. Accumulation of ethidium bromide in the *Salmonella* Typhimurium SL1344 $\Delta 4PAP \Delta acrF$ strain complemented with mutated versions of AcrE. Data represented are the mean of three biological replicates showing maximum RFU values after 30 min of ethidium bromide exposure \pm standard deviation. The annotation above indicates the mapping of each mutation to its binding box and the domain mapping of respective boxes. Data were analysed by one-way ANOVA and compared to the WT AcrE complement strain using Dunnett's test. Strains with significantly different ethidium bromide accumulation are indicated with **** ($P \leq 0.0001$). MPD, membrane-proximal domain.

on substrates utilising CH1 and CH2^{29,34}, while substrates documented to utilise CH3, such as ethidium bromide and rhodamine 6G²⁸ appear relatively unaffected.

AcrB with impacted channel 3 function supports the role of K366 in ensuring productive efflux of channel 1 and channel 2 substrates. The above data, combined with the location of the K366D AcrA mutation, strongly suggests that it may affect substrates entering through CH1 and CH2, but not CH3. To further increase assay sensitivity and avoid interference from substrates that use CH1-3 promiscuously, such as ethidium bromide, we produced an AcrB mutation (A33W T37W N298W AcrB) that impacted CH3 function²⁸, which allows for better separation of efflux signal arising from CH1 and CH2. The AcrB CH3 mutation was previously shown to impact the export of PACs²⁸. In agreement, the AcrB CH3 mutation caused an intermediate level of ethidium bromide efflux impairment between that of the $\Delta 4PAP \Delta acrB$ strain and the WT AcrAB complement strain (Fig. 7). Furthermore, the AcrB CH3 mutation increased susceptibility to PACs (Table S4) and impaired growth in the presence of 32 $\mu\text{g mL}^{-1}$ ethidium bromide (Fig. S2). Importantly, when present in combination with the AcrB CH3 mutation, the K366D AcrA mutation caused further impairment of ethidium bromide efflux, to a level comparable to that of the $\Delta 4PAP \Delta acrB$ strain (Fig. 7). Antimicrobial susceptibility testing also showed that the combination of K366D AcrA and AcrB CH3 mutations increased susceptibility to AcrB-substrates compared to the K366D AcrA or AcrB CH3 mutations acting alone (Table S4).

Strain	MIC ($\mu\text{g mL}^{-1}$)														
	HMMD				LMMD				PAC						
	ERY	DOX	FA	NOV	CHL	CLI	MIN	LZD	ACR	BZK	BER	CV	EtBr	MB	R6G
WT	128	1024	1024	512	4	512	2	512	256	64	>1024	64	1024	1024	1024
Δ 4PAP	4	2	8	2	0.5	4	0.25	16	16	4	128	2	16	8	4
WT AcrA complement	<u>64</u>	<u>64</u>	<u>256</u>	<u>64</u>	<u>4</u>	<u>128</u>	<u>1</u>	<u>128</u>	<u>64</u>	<u>32</u>	<u>>1024</u>	<u>16</u>	<u>128</u>	<u>128</u>	<u>128</u>
F292V AcrA	4	2	8	2	0.5	4	0.25	16	16	4	128	2	16	8	4
Q311F AcrA	64	64	256	64	4	128	1	128	64	32	>1024	16	64	128	128
K366D AcrA	16	16	32	16	1	32	0.25	16	64	32	>1024	16	64	128	64

Table 1. Antimicrobial susceptibility of the *Salmonella* Typhimurium SL1344 Δ 4PAP strain complemented with F292V, Q311F or K366D AcrA to drugs with different physicochemical characteristics. Underlined values highlight values for the Δ 4PAP strain complemented with wild type AcrA (WT complement). Bold values are at least two-fold or more different than the parent strain. HMMD, high-molecular-mass drug; ERY, erythromycin; DOX, doxorubicin; FA, fusidic acid; NOV, novobiocin; LMMD, low-molecular-mass drug; CHL, chloramphenicol; CLI, clindamycin; MIN, minocycline; LZD, linezolid; PAC, planar aromatic cation; ACR, acriflavine; BZK, benzalkonium chloride; BER, berberine; CV, crystal violet; EtBr, ethidium bromide; MB, methylene blue; R6G, rhodamine 6G.

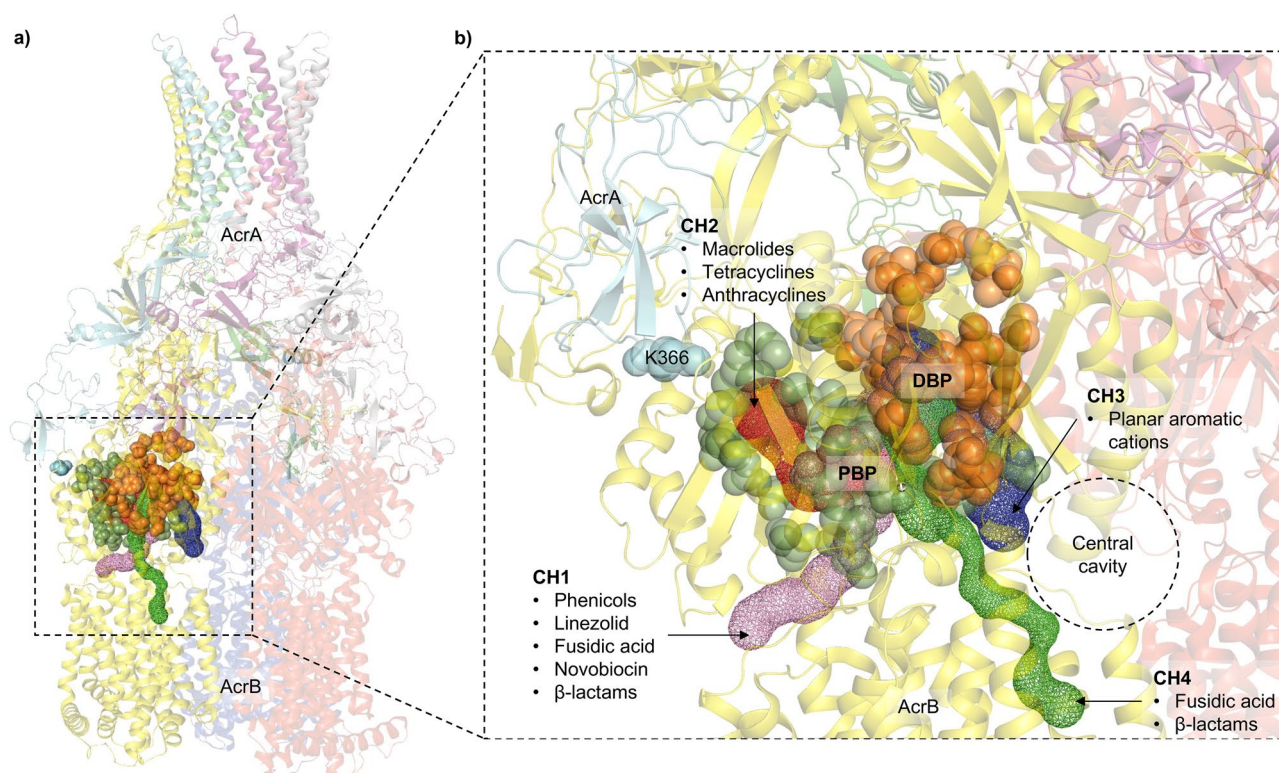


Figure 4. (a) The crystal structure of the trimeric AcrB transporter and the hexameric AcrA assembly (TolC not shown for clarity). The different substrate entry pathways are shown as coloured channels, and the binding pockets are indicated by coloured spheres. (b) Zoomed-in view of the substrate channels and the binding pockets relative to K366 of AcrA. The green and orange spheres correspond to the space-fill representation of the residues lining the proximal binding pocket (PBP) and the deep binding pocket (DBP), respectively. K366 is in the membrane-proximal domain of AcrA and impacts the residues lining the PBP and the entrance of channel 2 (CH2). Channel 1 (CH1) also feeds into the PBP, so is likely to be impacted by changes in K366. Channel 3 (CH3) starts from the central cavity and leads to the DBP. Similarly, channel 4 (CH4) starts from the groove formed by TM1/TM2 and leads to the DBP. Therefore, CH3 and CH4 are unlikely to be directly impacted by K366 substitutions.

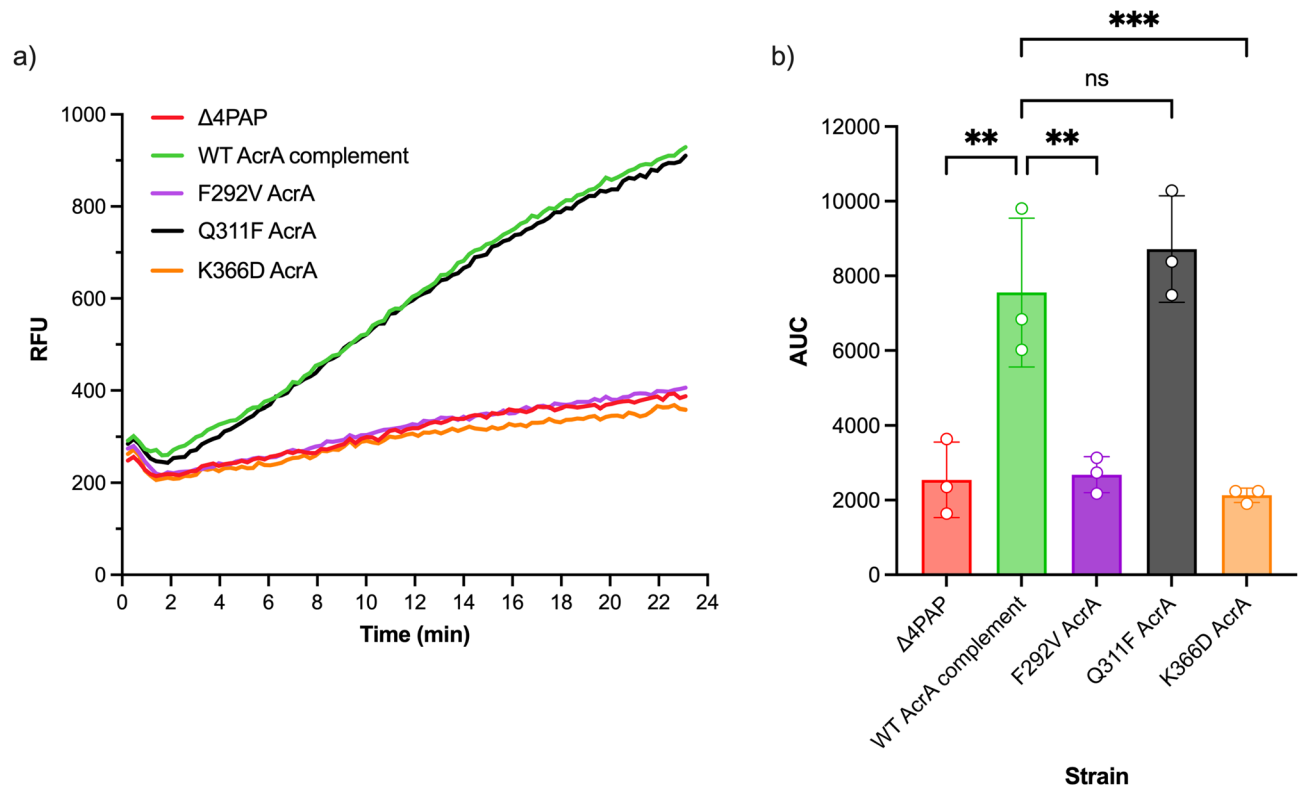


Figure 5. (a) Efflux of doxorubicin over time in the *Salmonella* Typhimurium SL1344 $\Delta 4PAP$ strain complemented with mutated versions of AcrA. Bacteria were treated with doxorubicin and the proton-motive force dissipater CCCP for one hour and then re-energised with glucose. Efflux was monitored by increasing RFU due to extracellular doxorubicin. Data presented are the mean of three biological replicates. (b) Area under curve (AUC) analysis for doxorubicin efflux over time. The data shown are the mean AUC of the three biological replicates shown in (a) \pm standard deviation. Data were analysed by one-way ANOVA and compared to the WT AcrA complement using Dunnett's test. Strains with significantly different AUC are indicated with ** ($P \leq 0.01$) or *** ($P \leq 0.001$). ns, not significant.

Next, the effect of the double mutation (K366D AcrA + AcrB CH3 mutation) on doxorubicin efflux was measured. WT AcrA combined with the AcrB CH3 mutation showed a similar level of doxorubicin efflux as the WT AcrAB complement, whilst the K366D AcrA mutation with WT AcrB resulted in impaired doxorubicin efflux. The double mutation caused complete impairment of doxorubicin efflux, like that of the $\Delta 4PAP \Delta acrB$ strain (Fig. 8). The doxorubicin efflux assay results were further validated by measuring the impact of the double mutation on growth in the presence of doxorubicin. The double mutation caused a growth defect in the presence of $2 \mu\text{g mL}^{-1}$ doxorubicin like the $\Delta 4PAP \Delta acrB$ strain. The K366D AcrA mutation with WT AcrB caused impaired growth in the presence of $8 \mu\text{g mL}^{-1}$ doxorubicin, whilst WT AcrA with the AcrB CH3 mutation did not affect growth (Fig. S3). The concentration-dependent effect of doxorubicin growth inhibition is consistent with the blockage of CH2, and gradual saturation of CH1, the function of which is partially impacted by the K366D AcrA mutation. Western blotting verified that the phenotypic effects of the AcrB CH3 mutation were not due to changes in protein expression or stability (Fig. S1). In summary, the AcrB CH3 disruption has a pronounced additive effect compared to the K366D AcrA mutation acting on its own, consistent with the role of the MPD of the PAP in the control of CH1- and CH2-substrates. These data further support the essential role that K366, and the MPD in general play in the transport of CH1- and CH2-substrates.

K366D also impacts channel 1 substrate transport. Like chloramphenicol, linezolid also uses CH1³⁴ and consistent with the interpretation that the K366D mutation impacts efflux through this channel, we observed a similar result for linezolid, with a pronounced concentration-dependent effect, which is most pronounced at $8 \mu\text{g mL}^{-1}$ and above (Fig. S4). This data suggests that K366 is also somehow involved in either active substrate vetting or surveillance of the substrate-bound state of the transporter, as discussed in detail in the section below.

Discussion

In this study, we set out to refine the previously reported “binding box” model of PAP-RND interaction²² by generating and characterising additional subtle and more conservative PAP mutations. Consistent with the model's prediction, we report that the AcrE residues that correspond to the previously identified critical residues in AcrA conserve their functional significance, as evidenced by targeted mutagenesis. Furthermore, we have been able to refine the effect of the previous, rather blunt mutations by separating previously reported double mutation

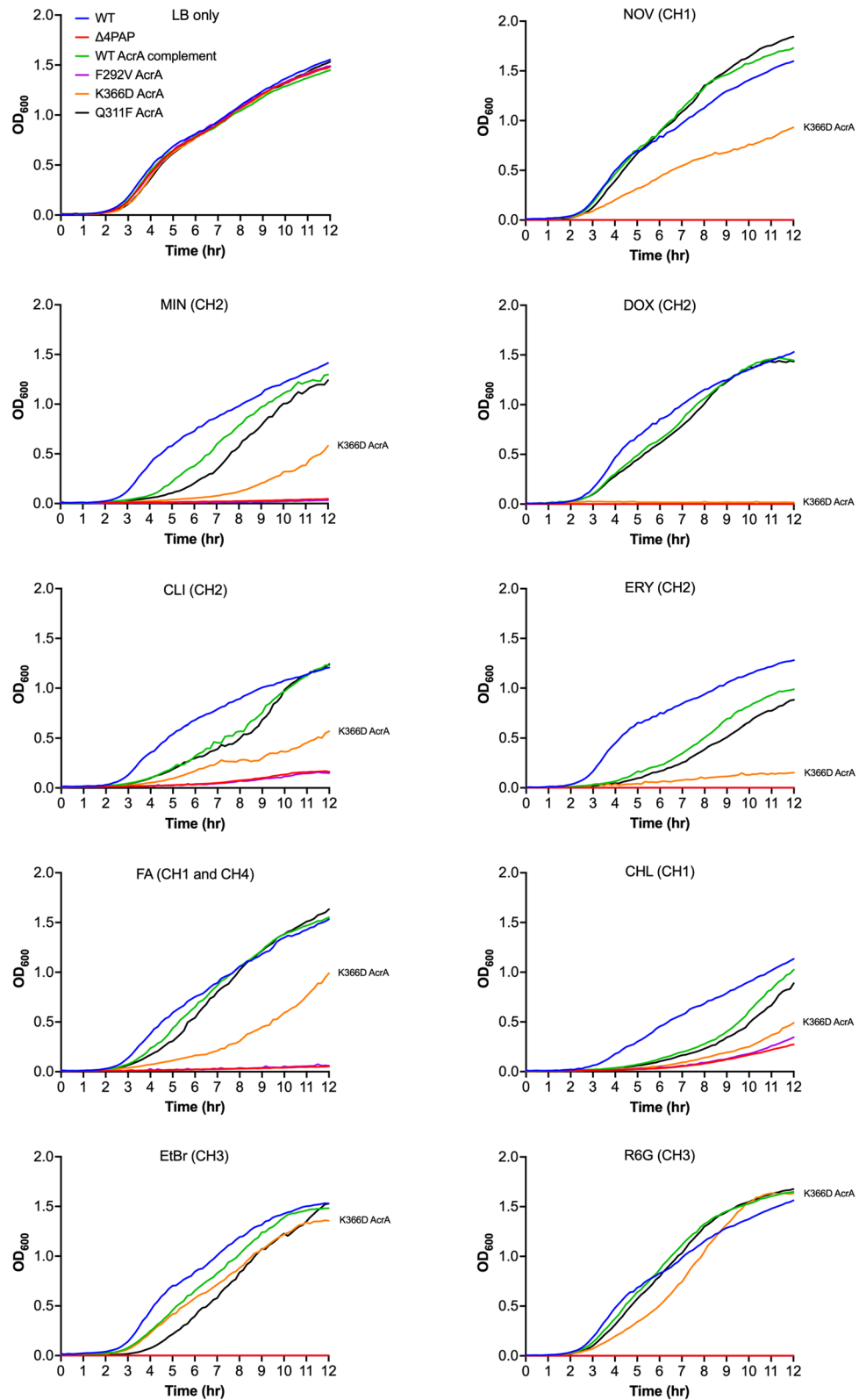


Figure 6. Growth kinetics of the *Salmonella* Typhimurium SL1344 Δ 4PAP strain complemented with mutated versions of AcrA. Abbreviations and concentrations of drugs used: CHL, $0.5 \mu\text{g mL}^{-1}$ chloramphenicol; CLI, $8 \mu\text{g mL}^{-1}$ clindamycin; DOX, $4 \mu\text{g mL}^{-1}$ doxorubicin; EtBr, $16 \mu\text{g mL}^{-1}$ ethidium bromide; ERY, $4 \mu\text{g mL}^{-1}$ erythromycin; FA, $8 \mu\text{g mL}^{-1}$ fusidic acid; MIN, $0.25 \mu\text{g mL}^{-1}$ minocycline; NOV, $4 \mu\text{g mL}^{-1}$ novobiocin; R6G, $16 \mu\text{g mL}^{-1}$ rhodamine 6G. Brackets indicate the preferred channel utilised by the substrate: CH1, channel 1; CH2, channel 2; CH3, channel 3; CH4, channel 4. The data shown are the mean OD_{600} values of three biological replicates. Concentrations of drugs are $0.25 \times \text{MIC}$ of K366D AcrA.

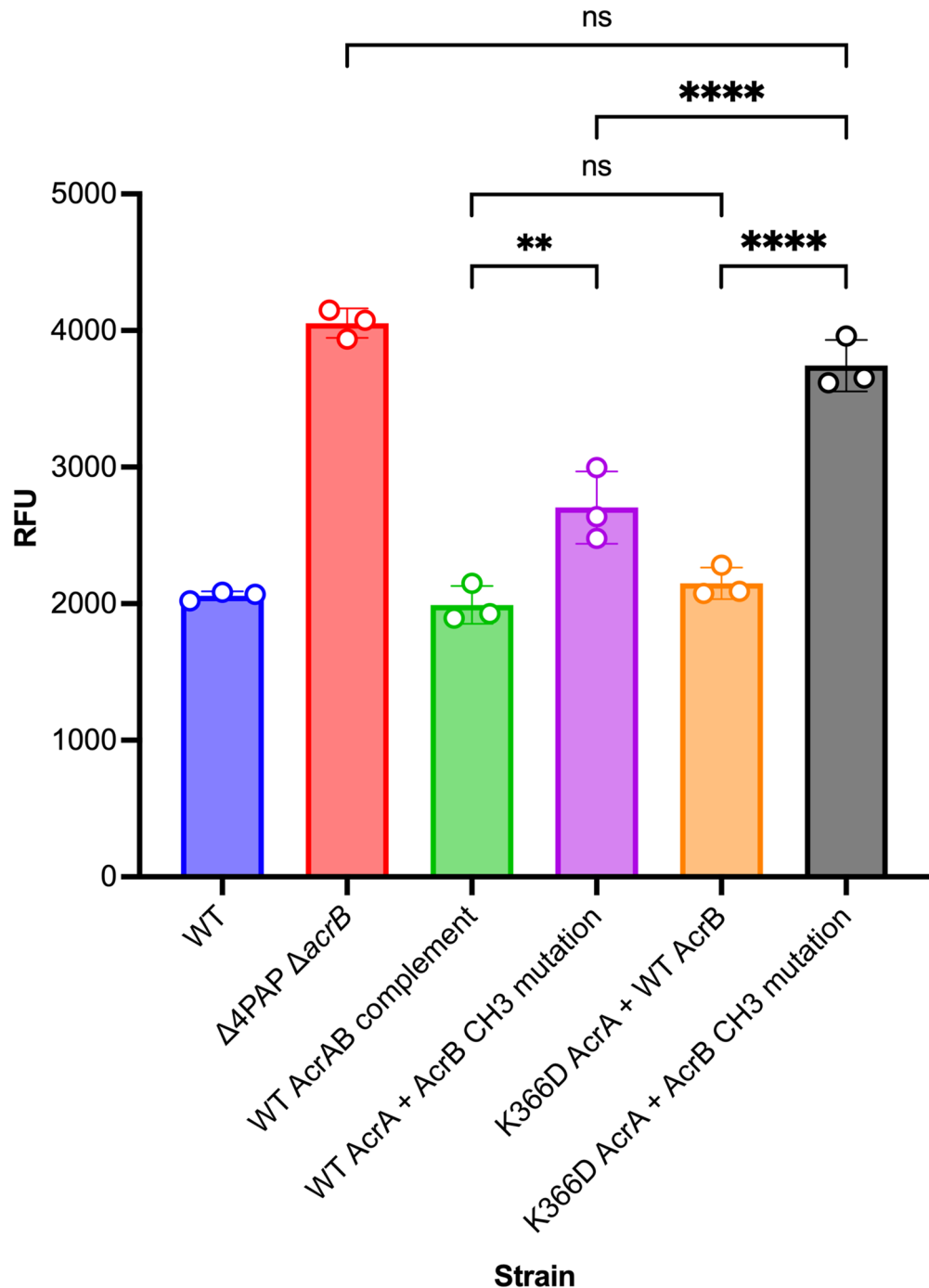


Figure 7. Accumulation of ethidium bromide in the *Salmonella* Typhimurium SL1344 Δ 4PAP Δ acrB strain complemented with K366D AcrA and AcrB channel 3 (A33W T37W N298W AcrB) mutation. The data shown are the mean of three biological replicates showing maximum RFU values after 30 min of ethidium bromide exposure \pm standard deviation. Data were analysed by one-way ANOVA and corrected for multiple comparisons using Tukey's test. Strains with significantly different ethidium bromide accumulation are indicated with ** ($P \leq 0.01$) or **** ($P \leq 0.0001$). ns, not significant.

T270F-T271F AcrA into T270A, T270D, T271A and T271D AcrA, which enabled us to narrow down T271 as a crucial residue for efflux function. Likewise, the function of F292 also seems to be critical for efflux function, with even subtle mutations (F292V AcrA) resulting in complete destabilisation of the AcrAB-TolC assembly. The R59A mutation, which is in proximity to G58, resulted in intermediate impairment of efflux function, validating the previously reported role for box 1, and the PAP β -barrel domain in the functional tripartite pump assembly.

During the refinement of the binding box 9, which maps to the MPD of the PAP, we identified an AcrA mutation (K366D) with a peculiar phenotype. The K366D mutation had no impact on ethidium bromide efflux

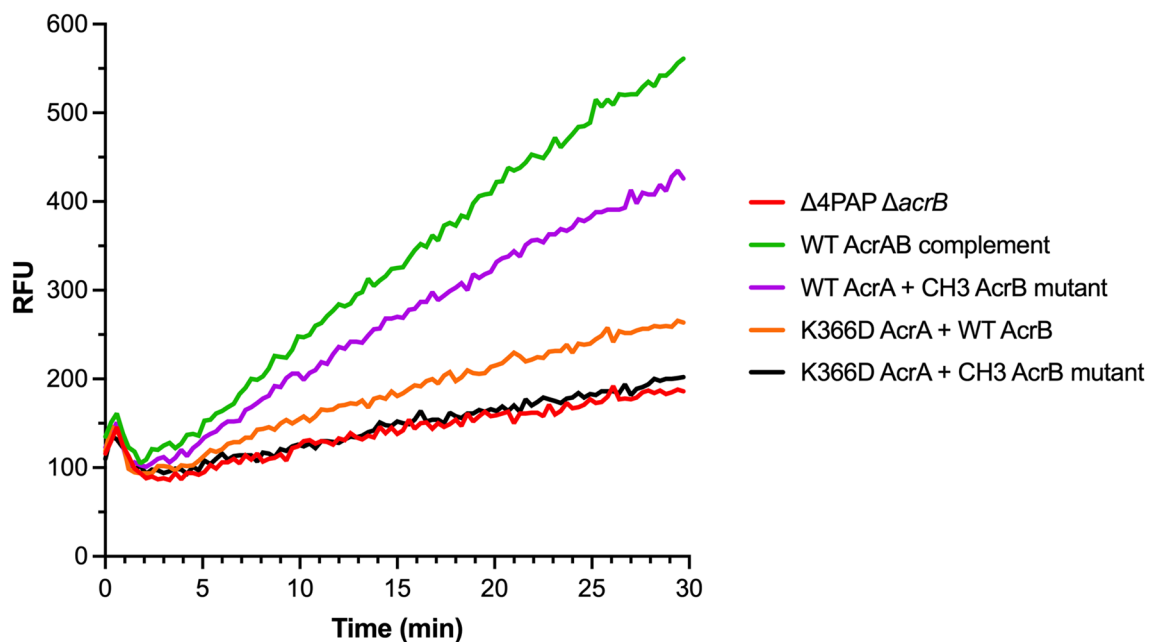


Figure 8. Efflux of doxorubicin over time in the *Salmonella* Typhimurium SL1344 $\Delta 4\text{PAP } \Delta\text{acrB}$ strain complemented with K366D AcrA and the AcrB channel 3 (CH3) mutation. Bacteria were treated with doxorubicin and the proton-motive force dissipater CCCP for 1 h and then re-energised with glucose. Efflux was monitored by increasing RFU due to extracellular doxorubicin. Data presented are the mean of three biological replicates. AcrB CH3 mutation refers to A33W T37W N298W AcrB.

or susceptibility to PACs. However, it significantly increased susceptibility to HMMDs and LMMDs compared to the WT AcrA complement. Structural analysis of the available RND tripartite assemblies^{20,31,32} indicated that K366 is in proximity to the proposed entry of CH2 (Fig. 4). We hypothesised that if this were indeed the case, as substrates and drugs exhibit clear channel access preferences, the K366D mutation will disproportionately affect substrates using CH1 and CH2, but not CH3 or CH4. Consistent with this prediction, we observed that the K366D AcrA mutation caused poor efflux of doxorubicin, a CH2-substrate. Furthermore, the K366D AcrA mutation caused a growth defect in the presence of several additional CH1-substrates (chloramphenicol, fusidic acid, and linezolid), as well as CH2-substrates (doxorubicin, erythromycin, and minocycline), but not CH3-substrates (ethidium bromide and rhodamine 6G).

Notably, the disruption of CH3 in AcrB had a pronounced additive effect on the K366D AcrA mutation acting in a WT AcrB background, consistent with the role of the PAP MPD in the control of CH1 and CH2 access to the respective substrates. Intriguingly, in addition to the straightforward effect of the K366D AcrA mutation on CH2 entry, the linezolid data presented here suggests that there is also a measurable impact on access of CH1-substrates to AcrB. This necessarily requires some level of allosteric communication, because K366 is too far from the proposed entrance of CH1^{28,29,40}.

At this stage, the available data doesn't provide a definitive answer as to how the MPD of the PAP may impact the apparent substrate preference and selection. However, the analysis of the available PAP-RND complex structures^{20,31,32} (Fig. 4), provides hints to the possible mechanism of the K366 action. One straightforward possibility, based on the location of K366 near the suggested entry of CH2²⁸, and the flexibility of its side-chain is that it may affect CH2-substrate access and kinetics by playing the role of a "cap" on the tunnel entrance, possibly sensing, and even partially coordinating the incoming substrate. However, the effect of the K366D AcrA mutation also extends to CH1-substrates, such as linezolid and chloramphenicol, while K366 is located too far away from the suggested CH1 entry points to be directly involved in any active substrate vetting. Thus, it is tempting to suggest that the K366 and the MPD as a whole may be involved in more generalised sensing of the substrate occupied state of the PBP (which is the convergence of CH1 and CH2)^{29,40}, and/or the potential propagating of the "substrate-occupied" signal upwards via a conformational change in the PAP leading to TolC engagement and channel opening as previously suggested⁸. Strikingly, this interpretation is directly supported by the very recent in situ cryo-electron tomography structure of the assembled AcrAB-TolC pump⁴¹, which displays strong and differential association of the MPDs of PAP protomers I and II with the PC1 and PN1/PC2 domains of AcrB respectively, with the latter in particular suggested to be associated with sensing the MBX3132 drug-occupied state of the transporter and providing a conformational signal to TolC, affecting its channel gating. Additionally, for the first time, the in-situ structure also unambiguously identifies the location of the C-terminal helices and the membrane-associated N-terminal tails of AcrA⁴¹, that appear to occupy a crevasse on the AcrB-surface that may also plausibly account for CH1 effects reported here, possibly providing additional sensory/allosteric input. Such sensory input may be allosterically conveyed to the engagement of the OMF partner protein during the initial assembly of the tripartite complex, or possibly provide directionality of the L-T-O transition during the efflux cycle, which is compatible with the mechanistic model of RND pump cycling suggested recently⁸.

In summary, we have identified the critical residues that drive PAP-RND recognition and describe a potential role for the PAP MPD in modulating substrate access to RND-transporters. These newly identified residues present novel drug target sites for the development of efflux inhibitors to tackle the growing threat of antimicrobial resistance.

Materials and methods

Bacterial strains and growth conditions. All strains were derived from *Salmonella enterica* serovar Typhimurium strain SL1344 (henceforth referred to as *S. Typhimurium*), a pathogenic strain first isolated from an experimentally infected calf⁴². All strains were grown in LB broth at 37 °C with aeration.

Growth kinetic assays. Overnight cultures ($\sim 10^9$ CFU mL⁻¹) of test strains were diluted to a starting inoculum of 10^6 CFU mL⁻¹ in a 96-well plate. Where appropriate, the test strains were diluted in LB broth supplemented with antibiotics. Growth was monitored over 12 h in a FLUOstar OMEGA plate reader (BMG Labtech, Germany).

Site-directed mutagenesis. Mutations in AcrA was generated using the plasmid *pacrA* (pET-20b (+) carrying the *acrA* gene from *S. Typhimurium* SL1334 with C-terminal 6xHis-tag). Mutations in both AcrA and AcrB was generated using the plasmid *pacrAB* (pET-20b (+) carrying the *acrAB* operon from *S. Typhimurium* SL1334 with a C-terminal 6xHis-tag). Mutations in AcrE were generated using the plasmid *pacrE* (pTrcHis2-TOPO carrying the *acrE* gene from *S. Typhimurium* SL1334 with a C-terminal 6xHis-tag). All site-directed mutagenesis (SDM) reactions were carried out using the QuikChange Lightning SDM Kit (Agilent, USA). The mutations were verified by sequencing (Eurofins Genomics, UK). Primers used for all the SDM reactions are listed in Table S1.

Ethidium bromide accumulation and efflux assay. The efflux activity of strains was assessed by measuring ethidium bromide accumulation and efflux as previously described⁴³.

Doxorubicin efflux assay. Doxorubicin efflux was measured similarly to ethidium bromide efflux, with some changes. Cells were grown to an OD₆₀₀ of 0.6 and washed with efflux buffer (20 mM potassium phosphate buffer with 5 mM magnesium chloride) three times. Carbonyl cyanide *m*-chlorophenylhydrazone (CCCP) and doxorubicin were added at a final concentration of 100 μM and 20 μM, respectively. Cells were incubated at 37 °C with aeration for 1 h. Following incubation, cells were washed with efflux buffer three times. Cells were energised with 25 mM glucose and doxorubicin efflux was measured over 30 min at excitation and emission wavelengths of 485 and 620–10 nm, respectively, in a FLUOstar OMEGA plate reader (BMG Labtech, Germany).

Antimicrobial susceptibility. The agar doubling dilution method was used to determine the minimum inhibitory concentrations (MICs) of various antimicrobials and dyes according to Clinical and Laboratory Standards Institute guidance⁴⁴. All MICs were repeated at least three times.

Western blotting. Wild-type and mutant AcrA were expressed in the *Salmonella Typhimurium* SL1344 Δ4PAP strain from *pacrA* plasmids. Wild-type and mutant AcrE were expressed in the *Salmonella Typhimurium* SL1344 Δ4PAP Δ*acrF* strain from *pacrE* plasmids. Wild-type and mutant AcrB were expressed in the *Salmonella Typhimurium* Δ4PAP Δ*acrB* strain from *pacrAB* plasmids. Cultures were grown to an OD₆₀₀ of 0.4 without induction. Cells were harvested and lysed in 10 mM Tris-HCl, 1 mM disodium EDTA, pH 8.0, supplemented with complete EDTA-Free Protease Inhibitor tablets (Roche, Switzerland) and 100 μg mL⁻¹ lysozyme using sonication. Membrane fractions were harvested, separated using a 12% SDS-PAGE gel for AcrA and AcrE and 8% SDS-PAGE gel for AcrB, and transferred to a PVDF membrane. The His-tagged proteins were blotted using a 1:5000 concentration of anti-6x His tag HRP-conjugated monoclonal antibody (Invitrogen, USA) and detected using Clarity Western ECL Substrate (Bio-Rad, USA) on an Amersham 680 Imager (Cytiva, USA).

Molecular visualisation of substrate channels. The location of the substrate channels 1–3 within the RND-transporter AcrB were calculated using CAVER software version 3.0⁴⁵ as described previously²⁸. For visualisation of the recently reported channel 4, the residues reported by Tam et al.³⁴ were used as starting coordinates. PyMOL (Molecular Graphics System, version 2.0 Schrödinger, LLC)⁴⁶ was used for 3D rendering of molecular structures and the substrate channels discussed.

Statistical analysis. Experiments were carried out at least three times on separate occasions. Data shown are the mean of at least three biological replicates, and where shown, error bars indicate standard deviations. All statistical comparisons were performed using one-way ANOVA with multiple comparison testing using Graph-Pad Prism version 9.2 for MacOS, San Diego, California USA, <http://www.graphpad.com>. Only *P*-values less than or equal to 0.05 were considered statistically significant.

Data availability

The authors confirm that the data supporting the findings of this study are available within the article and its supplementary materials.

Received: 19 October 2021; Accepted: 14 March 2022

Published online: 19 March 2022

References

- Ventola, C. L. The antibiotic resistance crisis: Part 1: causes and threats. *Pharm. Ther.* **40**, 277–283 (2015).
- Blair, J. M., Webber, M. A., Baylay, A. J., Ogbolu, D. O. & Piddock, L. J. Molecular mechanisms of antibiotic resistance. *Nat. Rev. Microbiol.* **13**, 42–51 (2015).
- Du, D. *et al.* Multidrug efflux pumps: Structure, function and regulation. *Nat. Rev. Microbiol.* **16**, 523–539 (2018).
- Colclough, A. L. *et al.* RND efflux pumps in Gram-negative bacteria; regulation, structure and role in antibiotic resistance. *Future Microbiol.* **15**, 143–157 (2020).
- Li, X. Z., Plesiat, P. & Nikaido, H. The challenge of efflux-mediated antibiotic resistance in Gram-negative bacteria. *Clin. Microbiol. Rev.* **28**, 337–418 (2015).
- Zwama, M. & Nishino, K. Ever-adapting RND efflux pumps in gram-negative multidrug-resistant pathogens: A race against time. *Antibiotics* **10**, 774 (2021).
- Neuberger, A., Du, D. & Luisi, B. F. Structure and mechanism of bacterial tripartite efflux pumps. *Res. Microbiol.* **169**, 401–413 (2018).
- Alav, I. *et al.* Structure, assembly, and function of tripartite efflux and type 1 secretion systems in gram-negative bacteria. *Chem. Rev.* **121**, 5479–5596 (2021).
- Nishino, K. & Yamaguchi, A. Analysis of a complete library of putative drug transporter genes in *Escherichia coli*. *J. Bacteriol.* **183**, 5803–5812 (2001).
- Nishino, K., Latifi, T. & Groisman, E. A. Virulence and drug resistance roles of multidrug efflux systems of *Salmonella enterica* serovar Typhimurium. *Mol. Microbiol.* **59**, 126–141 (2006).
- Zhang, Y. *et al.* The multidrug efflux pump MdtEF protects against nitrosative damage during the anaerobic respiration in *Escherichia coli*. *J. Biol. Chem.* **286**, 26576–26584 (2011).
- Horiyama, T. & Nishino, K. AcrB, AcrD, and MdtABC multidrug efflux systems are involved in enterobactin export in *Escherichia coli*. *PLoS ONE* **9**, e108642 (2014).
- Buckner, M. M. *et al.* Beyond antimicrobial resistance: evidence for a distinct role of the AcrD efflux pump in *Salmonella* biology. *MBio* **7**, e01916-16 (2016).
- Wang-Kan, X. *et al.* Lack of AcrB efflux function confers loss of virulence on *Salmonella enterica* serovar Typhimurium. *MBio* **8**, e00968-17 (2017).
- Wang-Kan, X. *et al.* Metabolomics reveal potential natural substrates of AcrB in *Escherichia coli* and *Salmonella enterica* Serovar Typhimurium. *MBio* **12**, e00109-21 (2021).
- Schaffner, S. H. *et al.* Extreme acid modulates fitness trade-offs of multidrug efflux pumps MdtEF-TolC and AcrAB-TolC in *Escherichia coli* K-12. *Appl. Environ. Microbiol.* **87**, e0072421 (2021).
- Nishino, K., Hayashi-Nishino, M. & Yamaguchi, A. H-NS modulates multidrug resistance of *Salmonella enterica* serovar Typhimurium by repressing multidrug efflux genes *acrEF*. *Antimicrob. Agents Chemother.* **53**, 3541–3543 (2009).
- Symmons, M. F., Marshall, R. L. & Bavro, V. N. Architecture and roles of periplasmic adaptor proteins in tripartite efflux assemblies. *Front. Microbiol.* **6**, 513 (2015).
- Du, D. *et al.* Structure of the AcrAB-TolC multidrug efflux pump. *Nature* **509**, 512–515 (2014).
- Wang, Z. *et al.* An allosteric transport mechanism for the AcrAB-TolC multidrug efflux pump. *Elife* **6**, e24905 (2017).
- Ge, Q., Yamada, Y. & Zgurskaya, H. The C-terminal domain of AcrA is essential for the assembly and function of the multidrug efflux pump AcrAB-TolC. *J. Bacteriol.* **191**, 4365–4371 (2009).
- McNeil, H. E. *et al.* Identification of binding residues between periplasmic adapter protein (PAP) and RND efflux pumps explains PAP-pump promiscuity and roles in antimicrobial resistance. *PLoS Pathog.* **15**, e1008101 (2019).
- De Angelis, F. *et al.* Metal-induced conformational changes in ZneB suggest an active role of membrane fusion proteins in efflux resistance systems. *Proc. Natl. Acad. Sci. USA* **107**, 11038–11043 (2010).
- Chacon, K. N., Mealman, T. D., McEvoy, M. M. & Blackburn, N. J. Tracking metal ions through a Cu/Ag efflux pump assigns the functional roles of the periplasmic proteins. *Proc. Natl. Acad. Sci. USA* **111**, 15373–15378 (2014).
- Lu, S. & Zgurskaya, H. I. MacA, a periplasmic membrane fusion protein of the macrolide transporter MacAB-TolC, binds lipopolysaccharide core specifically and with high affinity. *J. Bacteriol.* **195**, 4865–4872 (2013).
- Elkins, C. A. & Nikaido, H. Chimeric analysis of AcrA function reveals the importance of its C-terminal domain in its interaction with the AcrB multidrug efflux pump. *J. Bacteriol.* **185**, 5349–5356 (2003).
- Alav, I., Bavro, V. N. & Blair, J. M. A. Interchangeability of periplasmic adaptor proteins AcrA and AcrE in forming functional efflux pumps with AcrD in *Salmonella enterica* serovar Typhimurium. *J. Antimicrob. Chemother.* **76**, 2558–2564 (2021).
- Zwama, M. *et al.* Multiple entry pathways within the efflux transporter AcrB contribute to multidrug recognition. *Nat. Commun.* **9**, 124 (2018).
- Nakashima, R., Sakurai, K., Yamasaki, S., Nishino, K. & Yamaguchi, A. Structures of the multidrug exporter AcrB reveal a proximal multisite drug-binding pocket. *Nature* **480**, 565–569 (2011).
- Tam, H. K. *et al.* Binding and transport of carboxylated drugs by the multidrug transporter AcrB. *J. Mol. Biol.* **432**, 861–877 (2020).
- Glavier, M. *et al.* Antibiotic export by MexB multidrug efflux transporter is allosterically controlled by a MexA-OprM chaperone-like complex. *Nat. Commun.* **11**, 4948 (2020).
- Tsutsumi, K. *et al.* Structures of the wild-type MexAB-OprM tripartite pump reveal its complex formation and drug efflux mechanism. *Nat. Commun.* **10**, 1520 (2019).
- Mikolosko, J., Bobyk, K., Zgurskaya, H. I. & Ghosh, P. Conformational flexibility in the multidrug efflux system protein AcrA. *Structure* **14**, 577–587 (2006).
- Tam, H. K. *et al.* Allosteric drug transport mechanism of multidrug transporter AcrB. *Nat. Commun.* **12**, 3889 (2021).
- Schuster, S., Vavra, M. & Kern, W. V. Evidence of a substrate-discriminating entrance channel in the lower porter domain of the multidrug resistance efflux pump AcrB. *Antimicrob. Agents Chemother.* **60**, 4315–4323 (2016).
- Murakami, S., Nakashima, R., Yamashita, E. & Yamaguchi, A. Crystal structure of bacterial multidrug efflux transporter AcrB. *Nature* **419**, 587–593 (2002).
- Murakami, S., Nakashima, R., Yamashita, E., Matsumoto, T. & Yamaguchi, A. Crystal structures of a multidrug transporter reveal a functionally rotating mechanism. *Nature* **443**, 173–179 (2006).
- Zwama, M. & Yamaguchi, A. Molecular mechanisms of AcrB-mediated multidrug export. *Res. Microbiol.* **169**, 372–383 (2018).
- Daury, L. *et al.* Tripartite assembly of RND multidrug efflux pumps. *Nat. Commun.* **7**, 10731 (2016).
- Sennhauser, G., Amstutz, P., Briand, C., Storchenegger, O. & Grütter, M. G. Drug export pathway of multidrug exporter AcrB revealed by DARPIn inhibitors. *PLoS Biol.* **5**, e7 (2007).
- Chen, M. *et al.* In situ structure of the AcrAB-TolC efflux pump at subnanometer resolution. *Structure* **30**, 107–113 (2022).
- Wray, C. & Sojka, W. J. Experimental *Salmonella typhimurium* infection in calves. *Res. Vet. Sci.* **25**, 139–143 (1978).
- Smith, H. E. & Blair, J. M. Redundancy in the periplasmic adaptor proteins AcrA and AcrE provides resilience and an ability to export substrates of multidrug efflux. *J. Antimicrob. Chemother.* **69**, 982–987 (2014).

44. CLSI. *Performance standards for antimicrobial susceptibility testing, 30th edition*, 30th edn. Clinical and Laboratory Standards Institute (2020).
45. Brezovsky, J., Kozlikova, B. & Damborsky, J. Computational analysis of protein tunnels and channels. *Methods Mol. Biol.* **1685**, 25–42 (2018).
46. Schrödinger. The PyMOL Molecular Graphics System. 2.5.2 edn. Schrödinger LLC (2022).
47. Robert, X. & Gouet, P. Deciphering key features in protein structures with the new ENDscript server. *Nucleic Acids Res.* **42**, W320–324 (2014).

Acknowledgements

I.A. was funded by the Midlands Integrative Biosciences Training Partnership (MIBTP2) and grant BBSRC BB/M01116X/1 at the University of Birmingham. V.N.B. was supported by funding from BBSRC (grant BB/N002776/1). J.M.A.B. was funded by the BBSRC grant BB/M02623X/1 (David Phillips Fellowship to J.M.A.B.).

Author contributions

I.A. conducted the experiments. All authors designed the experiments and participated in the analysis and interpretation of data. V.N.B. and J.M.A.B. supervised the research. All authors wrote the paper and revised the manuscript.

Competing interests

The authors declare no competing interests.

Additional information

Supplementary Information The online version contains supplementary material available at <https://doi.org/10.1038/s41598-022-08903-9>.

Correspondence and requests for materials should be addressed to V.N.B. or J.M.A.B.

Reprints and permissions information is available at www.nature.com/reprints.

Publisher's note Springer Nature remains neutral with regard to jurisdictional claims in published maps and institutional affiliations.



Open Access This article is licensed under a Creative Commons Attribution 4.0 International License, which permits use, sharing, adaptation, distribution and reproduction in any medium or format, as long as you give appropriate credit to the original author(s) and the source, provide a link to the Creative Commons licence, and indicate if changes were made. The images or other third party material in this article are included in the article's Creative Commons licence, unless indicated otherwise in a credit line to the material. If material is not included in the article's Creative Commons licence and your intended use is not permitted by statutory regulation or exceeds the permitted use, you will need to obtain permission directly from the copyright holder. To view a copy of this licence, visit <http://creativecommons.org/licenses/by/4.0/>.

© The Author(s) 2022